RSC Advances

ROYAL SOCIETY OF CHEMISTRY

www.rsc.org/advances

Synthesis and Electromagnetic, Microwave Absorbing Properties of Polyaniline/Graphene Oxide/Fe_3O_4 Nanocomposites

Jing Zhao,[†] Junpin Lin,[‡] Junping Xiao,*[†] Huili Fan*[†]

The ternary composites of polyaniline/graphene oxide/Fe_3O_4 (PANI/GO/Fe_3O_4) were synthesized by a simple method and the electromagnetic absorption property of the composites was investigated in the paper. The structure of the composites were characterized with Fourier-transform infrared spectra, X-ray diffraction, Raman spectroscopy, X-ray photoelectron spectroscopy, and transmission electron microscope. It can be found that the maximum reflection loss of PANI/GO/Fe_3O_4 can reach -53.5 dB at 7.5 GHz, and the bandwidth exceeding -10 dB is 2.8 GHz with absorber thickness of 3.91 mm. The electromagnetic parameters indicated the enhanced electromagnetic absorption property of the nanocomposites was attributed to the better impedance matching. On the basis of the above characterization, an electromagnetic complementary theory was proposed to explain the impedance matching.

1 Introduction

With the increasing usage of electromagnetic wave devices, more and more electromagnetic interference (EMI) problems interfere with person's lives. Considerable theoretical and experimental research have been focused on designing and fabricating effective electromagnetic wave absorption materials with promising applications in electronic devices for commercial, industrial, and military affairs.[1-4] Because of the tremendous progress in absorbing stealth technology, EM-absorbing materials with a thin thickness, light weight, high reflection loss, and broad band are required.[5] However, the traditional microwave absorbing materials cannot meet all of the requirements such as to be strong, wide, lightweight and thin at the same time. A good way to overcome these problems is to develop composites.

Graphene oxide (GO) is a single sheet of graphite oxide bearing oxygen functional groups (i.e., epoxide, hydroxyl, carboxyl groups) on their basal planes and edges, and it can be synthesized by exfoliation of graphite oxide.[6] The tunable oxygen functional groups and good compatibility with polymer have made GO a promising material to synthesize functional nanocomposites.[7] GO has low density, in order to optimize the structure of the materials, making the materials with thin thickness and light weight, GO is often chosen as an integral part of the materials. It is well known that Fe_3O_4 nanoparticles have advantages for high-EM performance because they are typical soft metallic magnetic materials and show large magnetic anisotropy, good biocompatibility and low toxicity.[8-11]

PANI has received a great deal of attention because of their low cost, ease of synthesis and good environmental stability.[12-14] PANI can be used as a microwave absorbing material due to its high electrical conductivity. Therefore, the composites containing

PANI can be used as microwave absorbing materials which can increase the dielectric loss of composite materials.[15-20] Therefore the ternary composites of polyaniline/graphene oxide/Fe_3O_4 (PANI/GO/Fe_3O_4) were synthesized to make ideal comprehensive performance. However a toxic reducing agent in the reducing step is often used in synthesizing composites with GO.[1,2]

In this paper, we report a facile method to prepare PANI/GO/Fe_3O_4 composites without using toxic reducing agents. Although the synthesis didn't undergo the reducing step the composites still have good dielectric loss and magnetic loss, and they are also good for absorbing properties. The maximum reflection loss of the composites is -53.5 dB at 7.5 GHz and the bandwidth below -10 dB is 2.8 GHz (from 6.4 to 9.2 GHz) with thickness of 3.91 mm.

2 Experimental

2.1 Synthesis of Fe_3O_4 Microspheres

Fe_3O_4 microspheres were prepared according to a previous literature.[21] Briefly, 1.5 mol $FeCl_3$▪$6H_2O$ and 1 mol $FeCl_2$▪$4H_2O$ were dissolved in 100 mL of deionized water under mechanical stirring, and homogeneous yellow solution was obtained. Aqueous ammonia was added dropwise to the solution with violent mechanical stirring at 75□ for 0.5 h. The obtained black magnetite particles were washed with distilled water to remove the residues, and then the productions were vacuum dried at 45 □.

2.2 Synthesis of PANI/GO/Fe_3O_4 composites. Graphite oxide(GO) was synthesized by a modified Hummers' method.[21] PANI/GO/Fe_3O_4 composites were prepared as followed: 1mL of aniline and Fe_3O_4(1g) were added into 100mL solution which contains 0.25M $FeCl_3$ and 0.02M HCl, The mixture was stirred constantly in ice-water bath for 10h. 0.05g of GO treated by sonication and 10ml of APS (2.7 g) were added into the above solution for another 12h. The product was washed with distilled water several times until the filtrate became colorless. Then the productions were vacuum dried at 45□ for 24 h. For comparison purposes, PANI/GO and PANI/Fe_3O_4 were also prepared in similar procedures in the absence of Fe_3O_4 and GO.

2.3 Characterization Fourier transform infrared (FTIR) spectra were recorded on a NICOLET iS10. The crystal was characterized on X-ray diffraction (D/max 2550V, CuKαradiation).The morphology and size of the composites were characterized by field emission transmission electron microscope(FETEM: Tecnai F30 G^2). Raman spectroscopy was carried out on a Renishaw in Via Raman Microscope. The chemical states were investigated by X-ray photoelectron spectroscopy (XPS, AXIS ULTRA). The electromagnetic parameters were measured in a N5230C vector network analyzer. The samples were prepared by mixing the composites and paraffin wax at 50% weight fraction of each. The samples were pressed into a toroidal shape (φ_{out} 7.0mm; φ_{in} 3.0mm).

3 Results and discussion

The formation mechanism of PANI/GO/Fe_3O_4 composites is schematically depicted in Fig. 1. The composites were synthesized by a two-step method. In the first step oxidation process, Fe_3O_4 nanoparticles and aniline were added into the reaction system. The aniline monomer can immediately absorb on the surfaces of Fe_3O_4 by the electrostatic attraction. HCl and $FeCl_3$ were added into the suspension rapidly, the mixture was stirred at ice bath. $FeCl_3$ as an oxidizer oxidized aniline monomer to oligomers, which can make PANI oligomers uniform coated on the Fe_3O_4 nanoparticles surface.[20] Then in the second step oxidation process, GO was added into the suspension and Fe_3O_4 coated with PANI oligomers also can immediately absorb on the surfaces of GO by the electrostatic attraction. APS was added for further oxidation of the composites.

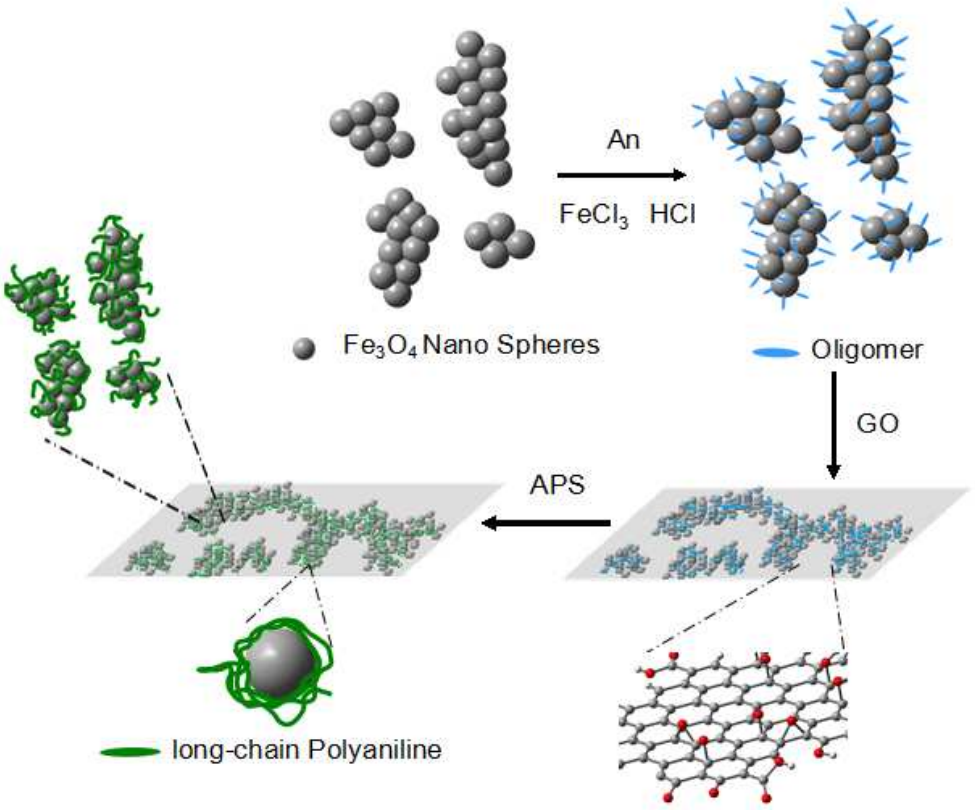

Fig. 1 Preparation procedure of PANI/GO/Fe_3O_4.

The spectrum (Fig. 2) of GO shows that the peaks at 3410 cm^{-1} can be identified as O—H stretching vibration of the association of carboxyl. The spectrum of GO also shows the presence of various oxygen-containing functional groups; characteristic peaks at 1730 and 1070 cm^{-1} have been assigned to carbonyl (CO) and epoxide (C-O-C) groups, respectively, and the peak at 1620 cm^{-1} arises due to the contributions from the skeletal vibrations of unoxidized graphitic domains or the remaining sp^2 carbon character of graphite.[23,24]

For the spectrum of PANI/GO/Fe_3O_4 nanocomposite, the peaks 1580 cm^{-1} and 1470 cm^{-1} in the literature are ascribed to the C=C/C—C stretching of the benzenoid and quinoid rings respectively. The peak at 1300 cm^{-1} is assigned to the C—N stretching of the secondary amine, a characteristic band of the conducting salt form of polyaniline originating from a bipolaron structure, related to the C—N stretching vibration. The band at 1120 cm^{-1} can be assigned to the in-plane bending vibration of the C—H (mode of N=Q=N, Q=N^+H—B, and B—N^+H=B), and the band at 806 cm^{-1} can be assigned to the out-of-plane deformation of C-H in 1,4-disubstituted benzene ring, which is formed during protonation.[25,26] The FTIR spectrum corresponds to a well-doped emeraldine salt. The shifting and merging of the band at 706 cm^{-1} (Fe—O stretching) confirms the composites contain Fe_3O_4.[27]

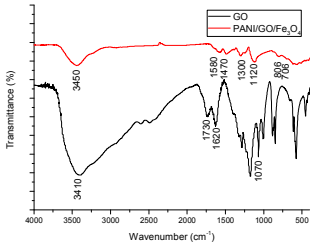

Fig. 2 FT-IR spectra of GO and PANI/GO/Fe_3O_4 nanocomposites.

Fig. 3a was the XRD pattern of graphene oxide, with a characteristic reflection plan (002) at 2θ=11.7°, indicating the d-spacing of 0.76 nm. This is attributed to intercalation of water molecules and generation of oxygenated functional groups such as epoxy and hydroxyl groups between the inter-galleries of the graphite sheets during severe oxidation. Disappearance of the reflection plane at (002) and merging of the planes of Fe_3O_4 and polyaniline show the good interfacial interaction between the planes. Nine peaks of PANI/GO/Fe_3O_4 (Fig. 3b) match well with the standard XRD data for (111), (220), (311), (400), (422), (511), (440), (533),and (731) planes of Fe_3O_4(JCPDS no.88-0315). Polyaniline doped HCl is semi-crystalline in nature as confirmed by the broad peaks at 2θ=19.795°(d=4.481Å) and 25.154°(d=3.537Å). [28,29]

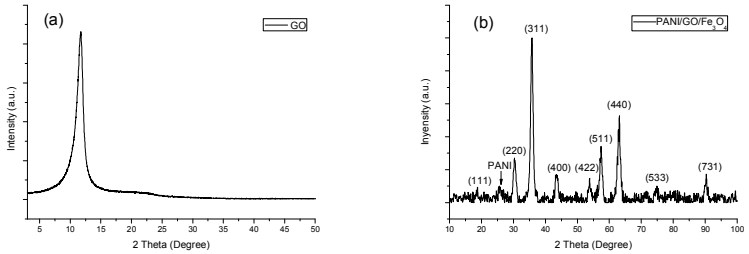

Fig. 3 (a) XRD pattern of GO ; (b) XRD pattern of PANI/GO/Fe_3O_4.

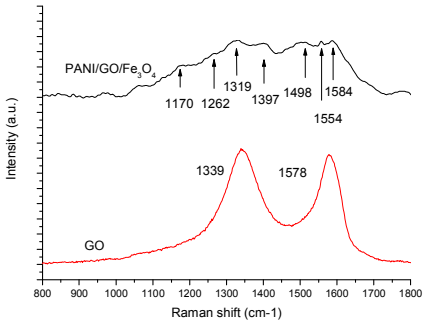

Fig. 4 Raman spectra of GO and PANI/GO/Fe_3O_4 nanocomposites.

The significant structural changes from GO to PANI/GO/Fe_3O_4 composites are also reflected in the Raman spectra, which confirms the interaction between polyaniline and GO. In Fig. 4, Raman spectra of GO exhibit two regular peaks, corresponding to the D-band line (about 1339 cm^{-1}) and the G-band line (about 1578 cm^{-1}). The G-band corresponds to the first-order scattering of the E_{2g} mode observed for sp^2 carbon domains, while the pronounced D band is caused by structural effects or edges that can break the symmetry and selection rule. For PANI/GO/Fe_3O_4 nanocomposites , the bands at 1170, 1262, 1397, 1498, and 1554 cm^{-1} indicating the presence of doped PANI structure are assigned to in-plane C-H bending of quinoid ring, in-plane C-H bending of benzenoid ring, C-C stretching of quinoid ring, C=C stretching of quinoid ring, and C=C stretching of benzenoid ring respectively. Compared with pristine GO, the G-band of graphene oxide in PANI/GO/Fe_3O_4 blue-shifted from 1578 cm^{-1} to 1584 cm^{-1}, suggesting the charge transfer from GO to PANI and Fe_3O_4.[23,25,27] Compared with GO, the position of the D-band of PANI/GO/Fe_3O_4 composites (about 1319 cm^{-1}) is gradually shifted to lower frequencies, which can be due to the fact that the electron pairs of the N atoms of PANI resonate with the adjacent benzene structure of GO.

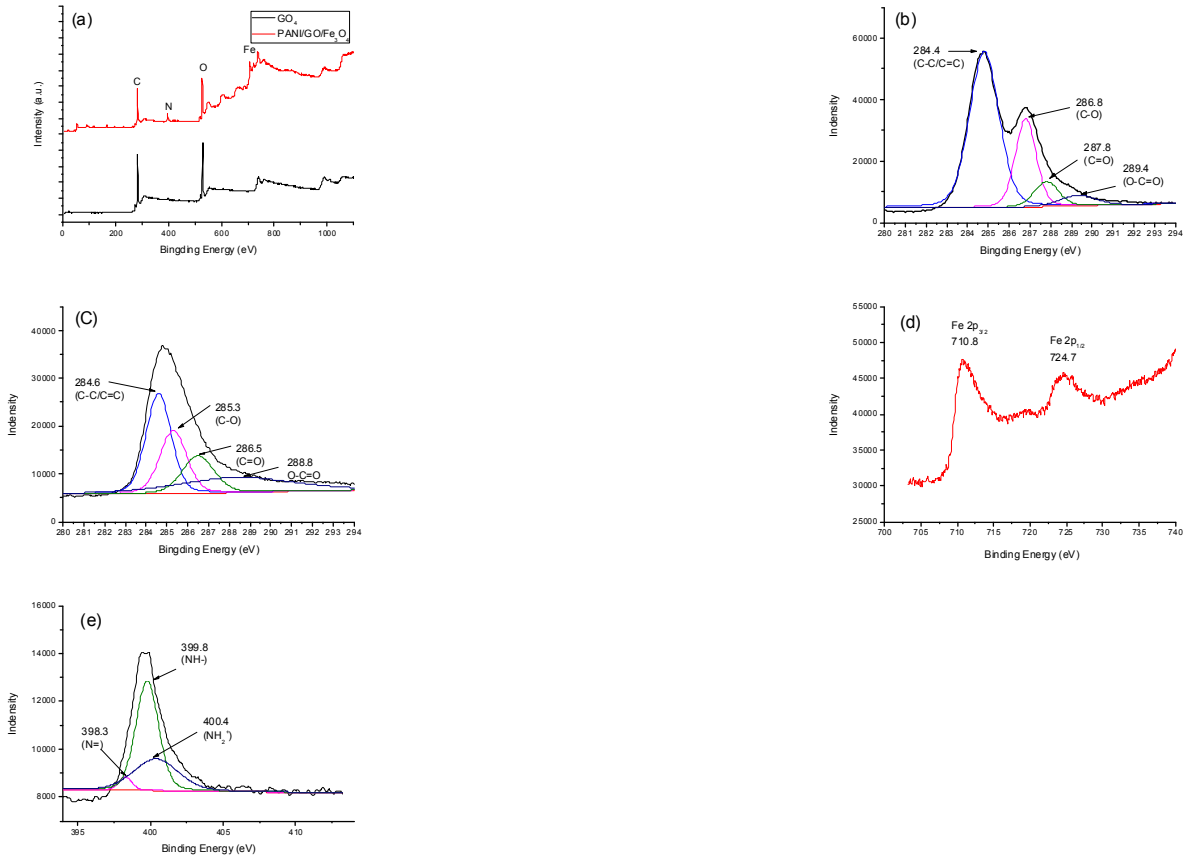

Fig. 5 (a) Survey scans for XPS spectra of GO, PANI/GO/Fe_3O_4 , nanocomposite. (b) C 1s peaks of GO (c) C 1s peaks of PANI/GO/Fe_3O_4 nanocomposite. (d) Fe 2p peaks of PANI/GO/Fe_3O_4 nanocomposite. (e) N 1s peaks of PANI/GO/Fe_3O_4 nanocomposite.

The XPS spectrum was used to further characterize the chemical composition of PANI/GO/Fe_3O_4. In the XPS spectra (Fig. 5a), the main peaks observed in the survey scans of the nanocomposites are C 1s, O 1s, N 1s and Fe 2p. Fig. 5b shows that the C 1s XPS spectra of GO deconvoluted into four different peaks. The peaks centered at 284.4, 286.8, 287.8, and 289.4 eV can be attributed to the C-C/C=C, C-O, or alkoxy, C=O and O-C=O groups respectively. The C 1s peaks of PANI/GO/Fe_3O_4 (Fig. 5c) became obviously weaker, which was probably accompanied by the formation of PANI/Fe_3O_4 composites.[23] Moreover, in the Fe 2p XPS spectrum of the PANI/GO/Fe_3O_4, the binding energy peaks at 710.75 and 724.65 eV agreed well with that of Fe $2p_{3/2}$ and Fe $2p_{1/2}$(Fig. 5d), respectively.[30] The high resolution scans for N 1s(Fig. 5e) in the PANI/GO/Fe_3O_4 composite could be grouped into three peaks at 398.28, 399.78 and 400.38 eV, corresponding to imine (N=), amine (NH), and protonated amine (NH_2^+) respectively.[31,27]

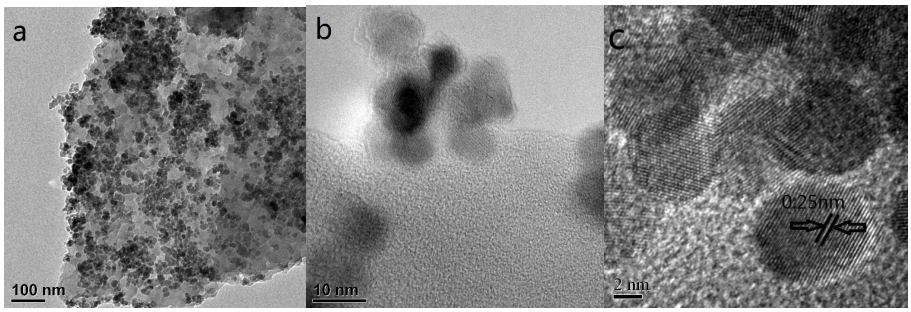

Fig. 6 (a) TEM and (b, c) HRTEM of PANI/GO/Fe_3O_4 nanocomposite.

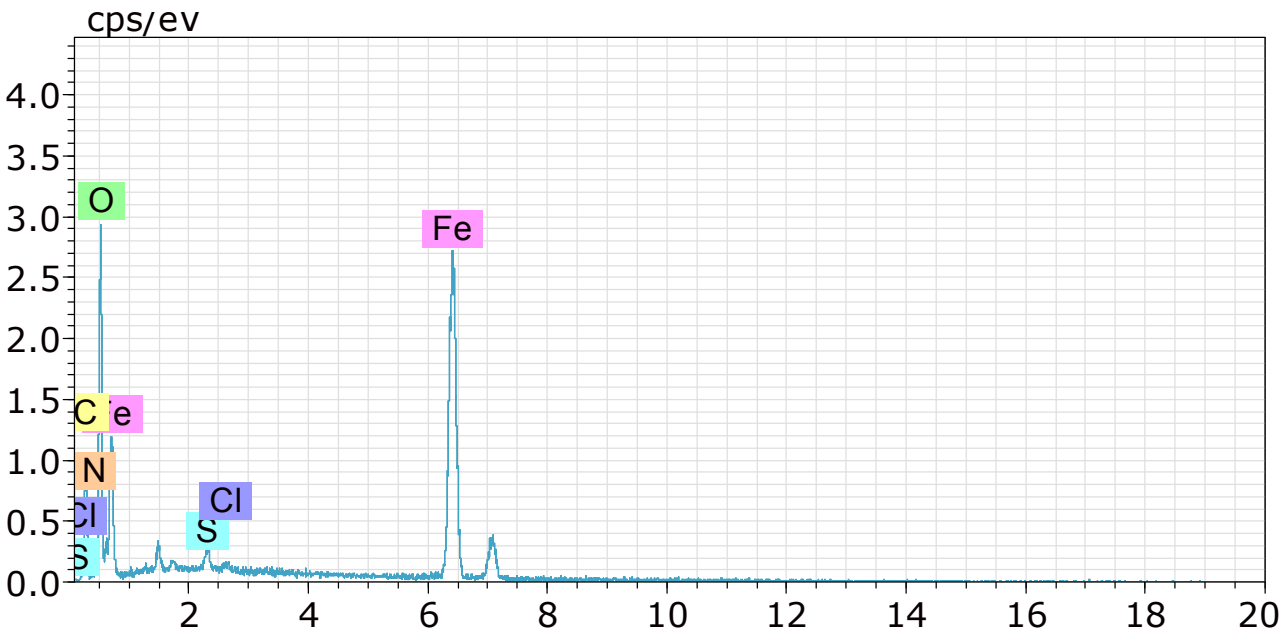

Fig. 7 EDS of PANI/GO/Fe_3O_4 nanocomposite.

The microstructure of the nanocomposites is analyzed with TEM, and the results are presented in Fig. 6. Fig. 6a reveals that Fe_3O_4 nanoparticles coated with PANI uniformly attached to the surface of the GO. The HRTEM image (Fig. 6b) of magnification of PANI/GO/Fe_3O_4 shows that Fe_3O_4 particles are coated with PANI with the average diameter between 10 and 20 nm, and PANI/ Fe_3O_4 particles are attached to GO. The well-defined lattice planes of Fe_3O_4 particles can be observed from Fig. 6c and the crystal lattice spacing(0.25 nm) can be attributed to the (311) plane of Fe_3O_4 particles, which is consistent with the result of XRD. The energy dispersive spectroscopy (EDS) as shown in Fig. 7 reveals that the sample is mainly composed of Fe, O, C, and N elements. There are S and Cl elements in the nanocomposites due to polyaniline doped with HCl and APS as oxidant oxidation polyaniline introduce into the nanocomposites

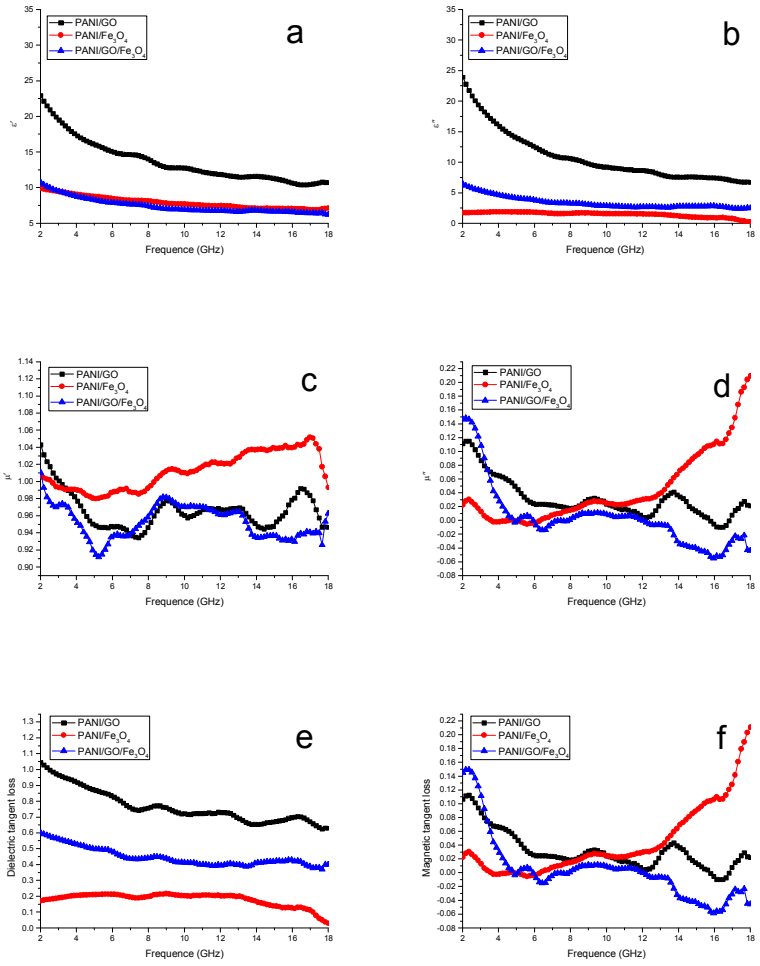

Fig. 8 Frequency dependence on real (a) and imaginary (b) parts of the complex permittivity of samples, real (c) and imaginary (d) parts of the complex permeability, and the corresponding dielectric (e) and magnetic loss tangents (f) of PANI/GO, PANI/Fe_3O_4 and PANI/GO/Fe_3O_4 composites.

The permittivity real part (ε'), permittivity imaginary part (ε''), permeability real part (μ'), permeability imaginary part (μ''), dielectric loss tangent (tan δε), and magnetic loss tangent (tanδμ) of the composites are presented in Fig. 8.

Fig. 8a shows that the ε' values of PANI/GO and PANI/GO/Fe_3O_4 decrease from 22.9 to 10.7 and 10.7 to 6.2, respectively, and their ε" values (Fig. 8b) vary from 23.9 to 6.7 and 6.4 to 2.4respectively, with the variation in the frequency range of 2-18 GHz. For PANI/Fe_3O_4, the values of its ε' (Fig. 8a) and ε" (Fig. 8b) negligibly decline from 9.9 to 7.1 and 1.7 to 0.2, respectively. Moreover, the figures above show that PANI/GO exhibits higher ε' and ε" values than other composites, this phenomenon may be due to the conducting polymers of PANI covered onto GO.

In Fig. 8c and 8d, the μ' and μ" values of all the composites exhibit complex fluctuations in the frequency range of 2-18 GHz. The μ' and μ" values of PANI/Fe_3O_4 are higher than that of other composites, there is a sign of magnetic ascension which is noticeable from the enhanced permeability, perhaps due to the specific weight of magnetic Fe_3O_4 particles is large than other composites. And it also can be seen that the μ" values of the composites are negative at high frequence, especially for PANI/GO/Fe_3O_4, which indicated that magnetic energy is radiated out from the composites which is due to the motion of charges. According to the Maxwell equations, the motion of charges in an electromagnetic field will produce an alternating electric field and induces a magnetic field.[9]

Fig. 8e and 8f show that the tan δε values of PANI/GO are higher than other composites, while its tan δμ values are lower than other composites. And the tanδμ values of PANI/Fe_3O_4 are higher than other composites, but the tanδε values is lower than that of other composites. The tanδε values of all composites are higher than the tanδμ values. The results suggest the electromagnetic attenuation mechanism of all composites is mainly attributed to dielectric loss.

As mentioned in the previous report,[32-38] the electromagnetic absorption property of absorber also depends on the combination between magnetic loss and dielectric loss. The dielectric loss and magnetic loss of PANI/GO are out of balance, thus the absorption of PANI/GO is weak. The dielectric loss and magnetic loss of PANI/Fe_3O_4 are small than other two materials, so it also have a weak absorption. Because Fe_3O_4 particles have magnetic characteristics and PANI have dielectric properties, the PANI/GO/Fe_3O_4 composites consisting of GO, PANI, and Fe_3O_4 nanoparticles may have better impedance matching, thus the PANI/GO/Fe_3O_4 composites will have an excellent electromagnetic absorption property. Firstly, dipole polarization is presented in Fe_3O_4 nanoparticles with nano size. The small size of Fe_3O_4 nanoparticles increase the dipole polarization, which contribute to dielectric loss. Secondly, the dielectric loss is related to the natural structure of Fe_3O_4.[39,40] Electronic polarization and ion polarization may take place during the electron transfer process between iron ions, which also has effect on the electromagnetic absorption property. Thirdly, at the interface of the ternary composites, interface defects can function as polarized centers and lead to an additional dielectric loss.[41] In addition, the better matching impedance also plays an important role in increasing the electromagnetic absorption property.[42,43] The PANI/GO/Fe_3O_4 showed the best absorption performance, which may be explained by a balance of two key factors, dielectric loss and magnetic loss. For PANI/GO,the high electromagnetic wave conversion capability was derived from a high tan δε, but the reflection coefficient was also high due to a high ε' value as a lot of electromagnetic wave was reflected back with a low absorption; for PANI/Fe_3O_4, the reflection of electromagnetic wave was not prominent, but the electromagnetic wave conversion capability was inferior, which also led to a decrease in absorption performance; for PANI/GO/Fe_3O_4 a balance was struck between the reflection and conversion of the electromagnetic wave, and

the best absorption performance was achieved as a result. From the above analyses, we can draw a conclusion that the electromagnetic absorption property of PANI/GO/Fe_3O_4 composites can be attributed to the efficient complementarities.

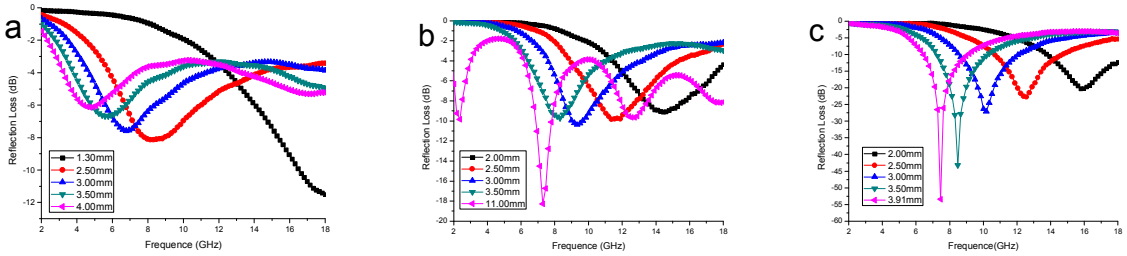

Fig. 9 The R_L of PANI/GO (a), PANI/Fe_3O_4 (b) and PANI/GO/Fe_3O_4 (c).

The reflection loss(R_L) values of the composites are calculated according to the following equations.

$$R_L(dB) = 20\log\left|\frac{Z_{in}-1}{Z_{in}+1}\right| \qquad (1)$$

$$Z_{in} = \sqrt{\mu_r/\varepsilon_r}\,\tanh\left[j(2\pi fd/c)\sqrt{\varepsilon_r\mu_r}\right] \qquad (2)$$

Where Z_{in} is the input impedance of the absorber, f is the frequency of electromagnetic waves, d is the thickness of the absorber, and c is the velocity of electromagnetic waves in free space.

Fig. 9a and 9b show that PANI/GO and PANI/Fe_3O_4 have same absorption properties. Each of them either has large dielectric loss or magnetic loss, it makes the dielectric loss and magnetic loss out of balance and not matching impedance. So they also have weak absorption properties. Compared with the composites above, PANI/GO/Fe_3O_4 composites with Core-Shell structure exhibit excellent microwave absorption properties (Fig. 9c). It can be found that the maximum R_L is down to -53.5 dB at 7.5 GHz and the absorption bandwidth exceeding -10 dB is 2.8 GHz (from 6.4 GHz to 9.2 GHz) with absorber thicknesses of 3.91mm. We find that 3.91mm is the perfect matching thickness, which is the quarter-wavelength matching layer, according to quarter-wavelength model.[44,45] This property can be applied to the coating absorbing materials, which can improve the absorbing effect.

The microwave absorption properties of core-shell structure nanocomposites are better than that of other composites due to its special structure. Fe_3O_4 nanoparticles coated with PANI effectively decreases the complex permittivity and increases the complex permeability, leading to improve characteristic impedances and magnetic loss abilities.[46,47] The consequent core/shell interfaces

will produce interfacial relaxation between Fe_3O_4 nanoparticles and PANI. And there also exist interfacial relaxation between PANI and GO. These are benefit to microwave absorption. The composites can improve dielectric loss through interface polarization and relaxation effects and reduce eddy effect and also increase anisotropy energy.

4 Conclusions

The paper has demonstrated an effective and versatile strategy to synthesize Fe_3O_4 coated with PANI loading on the GO. As a microwave absorbing materials, the PANI/GO/Fe_3O_4 nanocomposite exhibits excellent electromagnetic performance. The method presented in this work is very useful for enhancing the microwave absorption properties of these electromagnetic materials with high RL at the full-wave band of 1-18 GHz, which can be ascribed to the core-shell structure of Fe_3O_4 coated with PANI, the high dielectric loss and low density of GO, and the electromagnetic match in the microstructures. It was found that GO can be used to prepare absorbing materials, and its performance are as good as that of graphene. Its preparation is simple than that of graphene, and avoiding to stacking phenomenon in the reduction process. GO may become a promising material in absorbing materials. The method expands the potential application range of metal oxide nanomaterials used in microwave absorbing areas.

Acknowledgements
This work was supported by the State Key Lab of Advanced Metals and Materials of China 2013-ZD02.

Notes and references
†School of Chemistry and Biological Engineering, Department of Chemistry and Chemical Engineering, University of Science and Technology Beijing, Beijing 100083, China

‡State Key Laboratory for Advanced Metals and Materials, University of Science and Technology Beijing, Beijing 100083, China

1 B. Shen, W. T. Zhai, M. M. Tao, J. Q. Ling, W. G. Zheng, *ACS Appl. Mater. Interfaces*, 2013, **5**, 11383-11391.
2 G. H. Pan, J. Zhu, S. L. Ma, G. B. Sun, X. J. Yang, *ACS Appl. Mater. Interfaces*, 2013, **5**, 12716-12724.
3 P. B. Liu, Y. Huang, X. Sun, *ACS Appl. Mater. Interfaces,* 2013, **5**, 12355-12360.
4 G. H. Xu, N. Wang, J. Y. Wei, L. L. Lv, J. N. Zhang, Z. M. Chen, Q. Xu, *Ind. Eng. Chem. Res*., 2012, **51**, 14390-14398.
5 C. G. Hu, Z. Y. Mou, G. W. Lu, N. Chen, Z. L. Dong, M. J. Hu, L. T. Qu, *Phys. Chem. Chem. Phys*., 2013, **15**, 13038-13043.
6 K. Deepti, R. Kalyan, J. J. Shao, J. X. Huang, *ACS Nano*, 2014, **1**, 449-453.
7 F. Zhang, H. Q. Cao, D. M. Yue, J. X. Zhang, M. Z. Qu, *Inorg. Chem*., 2012, **51**, 9544-9551.
8 W. C. Zhou, X. J. Hu, X. X. Bai, S. Y. Zhou, C. H. Sun, J. Yan, P. Chen, *ACS Appl. Mater. Interfaces*, 2011, **3**, 3839-3845.
9 X. Sun, J. P. He, G. X. Li, J. Tang, T. Wang, Y. X. Guo, H. R. Xue, *J. Mater. Chem. C*, 2013, **1**, 765-777.
10 S. He, G. S. Wang, C. Lu, J. Liu, B. Wen, H. Liu, L. Guo, M. S. Cao, *J. Mater. Chem. A*, 2013, **1**, 4685-4692.
11 G. Z. Wang, Z. Gao, G. P. Wan, S. W. Lin, P. Yang, Y. Qin, *Nano Research* 2014, **7(5)**:704-716.
12 D. Zhao, X. Y. Guo, Y. Gao, F. Gao, *ACS Appl. Mater. Interfaces*, 2012, DOI:10.1021/am301484s.
13 S. Y. Lee, H. Lim, G. R. Choi, J. D. Kim, E. K. Suh, S. K. Lee, *J.Phys. Chem.C*, 2010, **114**, 11936-11939.
14 M. A. Dar, R. K. Kotnala, V. Verma, J. Shah, W. A. Siddiqui, Masood. Alam, *J. Phys. Chem. C*, 2012, **116**, 5277-5287.
15 D. D. Xu, Q. Xu, K. X. Wang, J. Chen, Z. M. Chen, *ACS Appl. Mater. Interfaces*, 2013, DOI: 10.1021/am404799.
16 Z. F. Li, H. Y. Zhang, Q. Liu, L. L. Sun, S. Lian, J. Xie., *ACS Appl. Mater. Interfaces*, 2013, **5**, 2685-2691.
17 Y. B. Sun, D. D. Shao, C. L. Chen, S. B. Yang, X. K. Wang, *Environ. Sci. Technol*., 2013, **47**, 9904-9910.
18 N. A. Kumar, H. J. Choi, Y. R. Shin, D. W. Chang, L. M. Dai, J. B. Beak, *ACS Nano*, 2012, **2**, 1715-1723.
19 S. G. Chen, Z. D. Wei, X. Q. Qi, L. C. Dong, Y. G. Guo, L. J. Wan, Z. G. Shao, L. Li, *J. Am. Chem. Soc*., 2012, **134**, 13252-13255.

20 G. Wu, K. L. More, C. M. Johnston, P. Zelenay, *Science,* 2011, DOI: 10.1126/science.1200832.
21 J. J. Jennifer, A. F. David, B. S. Matthew, S. Peter, E. W. Mary, *Nano Lett*., 2004, **4**, 719-723.
22 Z. Gao, Yang. W. L, Wang. J, Wang. B, Li. Z. S, Liu. Q, Zhang. M. L, *Energy Fuels*, 2013, **27**, 568-575.
23 M. Li, X. Y. Huang, C. Wu, H. P. Xu, P. K. Jiang, T. Tanaka, *J. Mater. Chem*., 2012, **22**, 23477-23484.
24 S. W. Zhang, W. Q. Xu, M. Y. Zeng, J. X. Li, J. Z. Xu, X. K. Wang, *Dalton Trans*., 2013, **42**, 13417-13424.
25 J. W. An, J. H. Liu, Y. C. Zhou, H. F. Zhao, Y. X. Ma, M. L. Li, M. Yu, *J. Phy. Chem. C*, 2012, **116**, 19699-19708.
26 M. Sawangphruk, M. Suksomboon, K. Kongsupornsak, J. Khuntilo, P. Srimuk, Y. Sanguansak, P. P. Klunbud, P. Suktha, P. Chiochan, *J. Mater. Chem. A*, 2013, **1**, 9630-9636.
27 K. Singh, A. Ohlan, V. H. Pham, R. Balasubramaniyan, S. Varshney, J. H. Jang, S. H. Hur, W. M. Choi, M. Kumar, S. K. Dhawan, B. S. Kong, J. S. Chung, *Nanoscale*, 2013, **5**, 2411-2420.
28 H. B. Gu, T. Sruthi, Y. D. Huang, A. C. Henry, Z. P. Luo, H. Neel, P. Y. David, S. Y. Wei, Z. H. Guo, *ACS Appl. Mater. Interfaces*, 2012, DOI: 10.1021/am301529t.
29 M. Zong, Y. Huang, Y. Zhao, X. Sun, C. H. Qu, D. D. Luo, J. B. Zheng, *RSC Adv*., 2013, **3**, 23638-23648.
30 C. L. Zhu, M. L. Zhang, Y. J. Qiao, G. Xiao, F. Zhang, Y. J. Chen, *J. Phys. Chem. C*, 2010, **114**, 16229-16235.
31 Y. Z. Li, X. Zhao, P. P. Yu, Q. H. Zhang, *Langmuir*, 2013, **29**, 493-500.
32 M. S. Cao, J. Yang, W. L. Song, D. Q. Zhang, B. Wen, H. B. Jin, Z. L.Hou, J. Yuan, *ACS Appl. Mater. Interfaces*, 2012, **4**, 6949-6956.
33 G. Li, T. S. Xie, S. L. Yang, J. H. Jin, J. M. Jiang, *J. Phys. Chem. C*, 2012, **116**, 9196-9201.
34 C. K. Cui, Y. C. Du, T. H. Li, X. Y. Zheng, X. H. Wang, X. J. Han, P. Xu, *J.Phys. Chem. B*, 2012, **116**, 9532-9531.
35 H. Zhang, A. J. Xie, C. P. Wang, H. S. Wang, Y. H. Shen, X. Y. Tian, *J. Mater. Chem. A*, 2013, **1**, 8547-8552.
36 X. F. Zhang, H. Huang, X. L. Dong, *J. Phys. Chem. C*, 2013, **117**, 8563-8569.
37 G. Z. Wang, Z. Gao, S. W. Tang, C. Q. Chen, F. F. Duan, S. C. Zhao, S. W. Lin, Y. H. Feng, L. Zhou, Y. Qin, *ACS Nano*, 2012, **12**, 11009-11017.
38 Y. P. Duan, Z. Liu, H. Jing, Y. H. Zhang, S. Q. Li, *J. Mater. Chem*., 2012, **22**, 18291-18299.
39 P. B. Liu, Y. Huang, *RSC Adv*., 2013, 19033-19039.
40 M. Fu, Q. Z. Jiao, Y. Zhao, H. S. Li, *J. Mater. Chem. A*., 2014, **2**, 735-744.
41 H. Guo, Y. Q. Zhan, Z. R. Chen, F. B. Meng, J. J. Wei, X. B. Liu, *J. Mater. Chem. A*, 2013, **1**, 2286-2296.
42 J. Yang, J. Zhang, C. Y. Liang, M. Wang, P. F. Zhao, M. M. Liu, J. W. Liu, R. C. Che, *ACS Appl. Mater. Interfaces*, 2013, **5**, 7146-7151.
43 Y. J. Chen, G. Xiao, T. S. Wang, Q. Y. Ouyang, L. H. Qi, Y. Ma, P. Gao, *J. Phys. Chem. C*, 2011, **115**, 13603-13608.
44 T. Wang, R. Han, G. G.Tan, J. Q. Wei, L. Qiao, F. S. Li, *Journal of Applied Physics* **112**, 104903 (2012).
45 F. Qin, C. Brosseau, *Journal of Applied Physics* **111**, 061301 (2012).
46 J. W. Liu, R. C. Che, J. J. Xu, M. M. Liu, Z. W. Liu, *J. Phys. Chem. C*, 2013, **117**, 489-495.
47 C. F. Maria, D. Dimitrios, M. S. Juleon, D. A. S. Laurens, *J. Phy. Chem. C*, 2013, **117**, 8032-8040.